

A PRACTICAL NUMERICAL APPROACH FOR LARGE DEFORMATION PROBLEMS IN SOIL

Y. HU AND M. F. RANDOLPH*

Geomechanics Group, Department of Civil Engineering, The University of Western Australia, Nedlands, WA 6907, Australia

SUMMARY

A practical method is presented for numerical analysis of problems in solid (in particular soil) mechanics which involve large strains or deformations. The method is similar to what is referred to as 'arbitrary Lagrangian–Eulerian', with simple infinitesimal strain incremental analysis combined with regular updating of co-ordinates, remeshing of the domain and interpolation of material and stress parameters. The technique thus differs from the Lagrangian or Eulerian methods more commonly used. Remeshing is accomplished using a fully automatic remeshing technique based on normal offsetting, Delaunay triangulation and Laplacian smoothing. This technique is efficient and robust. It ensures good quality shape and distribution of elements for boundary regions of irregular shape, and is very quick computationally. With remeshing and interpolation, small fluctuations appeared initially in the load-deformation results. In order to minimize these, different increment sizes and remeshing frequencies were explored. Also, various planar linear interpolation techniques were compared, and the unique element method found to work best.

Application of the technique is focused on the widespread problem of penetration of surface foundations into soft soil, including deep penetration of foundations where soil flows back over the upper surface of the foundation. Numerical results are presented for a plane strain footing and an axisymmetric jack-up (spudcan) foundation, penetrating deeply into soil which has been modelled as a simple Tresca or Von Mises material, but allowing for increase of the soil strength with depth. The computed results are compared with plasticity solutions for bearing capacity. The numerical method is shown to work extremely well, with potential application to a wide range of soil–structure interaction problems. © 1998 John Wiley & Sons, Ltd.

Int. J. Numer. Anal. Meth. Geomech., vol. 22, 327–350 (1998)

Key words: finite element analysis; large strain; remeshing; integration; penetration; bearing capacity

1. INTRODUCTION

In the past two decades, considerable effort has been expended on the numerical solution of problems involving large deformation or large strain. In finite element analysis, there are three main approaches to deal with continuum mechanics problems, namely the Eulerian, total Lagrangian and updated Lagrangian formulations.¹ A further approach has been developed more recently, that is referred to as an 'Arbitrary Lagrangian–Eulerian' (ALE) formulation. A full description of these methods has been covered in other publications.^{1,2} However, a brief summary is included here as background to the proposed approach.

*Correspondence to: M. F. Randolph, Geomechanics Group, Department of Civil Engineering, The University of Western Australia, Nedlands, WA 6907, Australia

In the Eulerian or spatial approach, attention is focused on the response within a fixed region of space as time passes. The method is well suited for the study of fluids and other homogeneous materials, particularly where there is no free boundary. However, in solid mechanics, it is more natural to adopt a Lagrangian approach, considering a given region of material, rather than the region of space which the material occupies momentarily. Since the governing equations of statics and dynamics refer directly to the solid matter (rather than a region of space), complex material and stress derivatives must be included in a Eulerian approach, which can render the finite element equations highly non-linear.³ As such, little effort has been devoted to Eulerian formulations for solid mechanics, although recent work on deep penetration problems has demonstrated the potential of this approach.⁴

Both Total Lagrangian (TL) and Updated Lagrangian (UL) descriptions⁵ are commonly used to deal with large displacements, rotations and strains of solids. The difference between the two approaches concerns the reference state for the body, which is taken at time zero in the TL approach, while the current (updated) geometry is used in the UL approach. In practice, the TL formulation is probably only useful for problems involving large deformations but small strains, or where a complex stress-strain law valid for large strains is to be followed. The UL formulation is more common, with the spatial position of the body updated with each deformation increment. In both approaches it is necessary to include second derivatives in the description of strains, in order to account for finite rotations of the body.

A serious limitation of the Lagrangian approaches is gross distortion of individual finite elements that accompanies large strains within the body. Zienkiewicz⁶ and Cheng and Kikuchi⁷ have described mesh rezoning techniques to circumvent the limitations associated with element distortion. However, complex contact boundary representation may still be impaired using an updated Lagrangian mesh.

In an attempt to overcome the limitations of the pure Lagrangian and Eulerian approaches, a more flexible approach called Arbitrary Lagrangian-Eulerian (ALE) has been developed by Ghosh and co-workers.^{2,8,9} The problem of element distortion can be avoided by uncoupling of nodal point displacements and material displacements. In essence, the extent to which stress and material properties 'stream' through the finite element mesh (Eulerian) or the mesh moves with the material (Lagrangian) may be varied arbitrarily. This approach has been employed to execute large deformation analysis of elastic-plastic solids by a variety of researchers.¹⁰⁻¹³

In geomechanics, a large strain theory in Lagrangian co-ordinates has been developed by Kioussis *et al.* and applied to cone penetration analysis.^{14,15} Because of the complex constitutive behaviour of soil, the final form of the yield condition in the Lagrangian description is rather complicated. The arbitrary Lagrangian-Eulerian formulation has been applied to modelling cone penetration in homogeneous and layered soils, by van den Berg *et al.*^{4,16} In that work, although the formulation is ALE, the final result uses a constant mesh, fixed to the cone penetrometer, with the soil streaming past the cone. As such, the analysis is essentially Eulerian. The approach is particularly suitable since there is no free surface (since only deep penetration is considered). In fact, the formal ALE approach still cannot easily deal with the free soil surface.

In the present paper, a finite element method that falls essentially within the ALE category is presented. Conventional finite element analysis with an infinitesimal strain model is combined with fully automatic mesh generation and plane linear stress interpolation techniques to deal with two-dimensional (and axisymmetric) large deformation problems in soil. Complete remeshing and interpolation of stress and material parameters is carried out typically every 10-20 increments. Since the accuracy of the solution increases with the number of increments, fast mesh

generation and interpolation methods are essential. As the soil deforms, the boundary can become more and more irregular, and so the generated mesh must be able to fit boundaries of arbitrary shape well. A simple planar interpolation technique for stresses and material properties has been found to be both efficient and of sufficient accuracy to preserve overall equilibrium.

Application of the method is illustrated by three surface penetration problems of gradually increasing complexity. First, a typical problem involving a strip footing on the soil surface, subjected to large settlement, is analysed with and without re-meshing, and the effect of increment size and remeshing frequency on the results are explored. Results are then presented for a cavity expansion, a strip footing (plane strain) and a spudcan foundation (axisymmetric) penetrating significantly into soil where the strength is assumed to vary linearly with depth. For all case, comparisons are presented with plasticity solutions, and it is shown that the method works extremely well on such large deformation problems.

2. MESH GENERATION

2.1. Overview of various mesh generation methods

The finite element method is a powerful and versatile means of numerical analysis, but its effectiveness can be hampered by the need to generate a mesh, which can be very time consuming to generate manually. For the present application, an efficient, automatic scheme is essential. In recent years, there has been a large amount of research into automating the discretization of geometric domains for the finite element method. A survey of mesh generation methods has been presented by Ho-Le.¹⁷ The most popular and common methods, using the classification terminology of Ho-Le, are listed below.

- (1) *Nodal connection approach.* This approach can be broken down into two steps. The first step is the placement of nodes within the domain of interest. The second step is the connection or triangulation scheme, such as Delaunay triangulation, used to connect the grid of nodes into a valid finite element mesh.

The techniques for automatic generation of nodes may be divided into random^{18–20} and non-random^{21,22} methods. Most of these methods mentioned are designed to produce triangular elements, with the exception of Lee's method which attempts to generate quadrilaterals.²³

- (2) *Grid-based approach.* Here the geometric domain is overlain with a grid scheme enclosing the domain. The grid is then subdivided, cut and adjusted to accommodate the domain boundaries. This approach was proposed by Thacker *et al.*²⁴ The techniques tend to produce well shaped elements in the interior of the mesh but sometimes have difficulty fitting element shapes on the boundaries, although this deficiency has been addressed by various researchers.^{25,26}
- (3) *Mapped element approach.* Mapping methods are based on the application of blending and shape functions across regular geometric patches to produce a mesh of elements in the patch.^{27,28} The major drawback of these techniques is that a complex domain must be subdivided by the user into simpler patches to which the mapping procedures may be applied; this limits the degree to which the method can be automated. Recent work applying artificial intelligence methods shows prospects of automating this domain subdivision process more fully.²⁹

- (4) *Decomposition approach.* This approach examines the domain to be meshed for geometries or topologies which can be removed from the domain as elements or regions which may be subdivided to form elements. Elements and/or regions are successively removed until the domain is completely meshed. This approach is based on either recursion³⁰ or iteration.^{31,32}

2.2. Fully automatic mesh generation method

A powerful mesh generation method has to be fully automatic, smooth and easy to control the density of mesh. The mesh generation method adopted here,³³ which falls into the nodal connection class (see above), includes three main techniques: mesh generation using normal offsetting, mesh smoothing, and application of an external mesh density function. These techniques, which make this method very powerful, are described below.

The mesh generation is divided into several steps. The first step generates a mesh representing the boundary geometry of the model. In the next step the interior region of the model is processed to produce an array of appropriately spaced nodes. This step is further broken down into two distinct processes: normal offsetting of the nodes on the current boundary (at the edge of the vacant region), and processing the resulting new points to determine new nodal locations. These processes are repeated until the domain has been filled, with an appropriate convergence criterion satisfied. Finally a Delaunay triangulation³⁴ makes appropriate element connections to form a finite element mesh.

Figure 1(a) shows the uniform mesh resulting from the Delaunay triangulation of the nodes produced by normal offsetting. It may be seen that a high proportion of the triangles contain a right-angle, rather than the optimum, which would be quasi-equilateral triangles. In order to adjust the element shapes, a mesh smoothing procedure is applied using the Laplacian technique such that:

$$x_i = \frac{1}{2N_i} \sum_{n=1}^{N_i} (x_{nj} + x_{nl}); \quad i = 1 \rightarrow I \quad (1)$$

$$y_i = \frac{1}{2N_i} \sum_{n=1}^{N_i} (y_{nj} + y_{nl}); \quad i = 1 \rightarrow I \quad (2)$$

The definitions of the variables in equations (1) and (2) are described in Figure 2, where N_i is the number of elements surrounding node i , I is the number of nodes inside the domain. Although problems exist with the Laplacian technique,³⁵ the good initial quality of the mesh that is produced by the normal offsetting process guarantees rapid convergence and good quality elements.

Figure 1(b) shows the same mesh as Figure 1(a), following the application of Laplacian smoothing. It can be seen that the elements in Figure 1(b) are more equilateral than those in Figure 1(a).

In order to optimize the accuracy of the analysis for a given total number of elements, it is necessary to control the mesh density. The mesh density function is decoupled from the actual mesh generation procedure. Thus, during any mesh generation, the local nodal spacings are determined by a query to an external function. Here, the mesh density function, f_d , has been taken as a simple exponential function of the distance, d , from a specified origin at (x_0, y_0) :

$$f_d = Ae^{Ed} \quad (3)$$

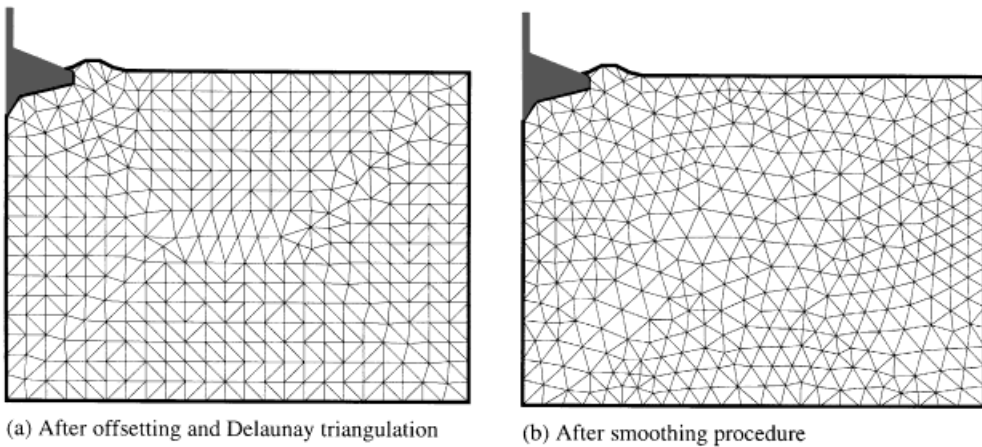
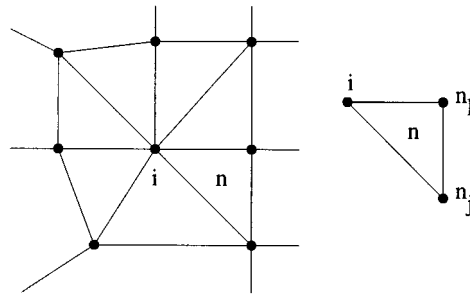


Figure 1. Uniform mesh of spudcan penetrating into soil

Figure 2. Neighbouring nodes to node i

where A and E are constants. The effect of applying a mesh density function may be seen in Figure 3.

Although the meshes used in the present paper have been generated using the above mesh density function from a user-specified origin, the approach would be very suitable for adaptive mesh generation, where the density function could be linked to a measure of the error in the finite element solution, or to a measure of the strain gradients.

The technique described here offers a fully automatic mesh generation method for finite element analysis, that is also very fast. The meshes shown in Figure 1(b) with 753 elements and Figure 3 with 532 elements took respectively only 2.47 and 1.41 CPU seconds on a DEC Alpha workstation.

The full mesh generation procedure for the finite element method described in this paper consists of four steps:

- (1) mesh generation with normal offsetting, smoothing and mesh density function;
- (2) transformation of three-node triangular elements to six-node triangular elements;

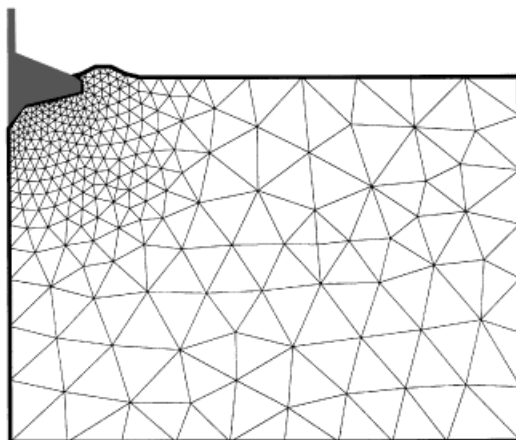


Figure 3. Non-uniform mesh of deformed domain

- (3) numbering the nodes of the mesh for finite element analysis;
- (4) writing a postscript file for plotting the mesh and the input data file to link with the AFENA³⁶ finite element analysis package.

For the case of strip footing response and pipeline penetration, a typical mesh with 2041 nodes and 982 six-node triangular elements (for example, mesh(c) shown later in Figure 9) took a total of only 64.3 CPU seconds on a SUN Sparc-ELC workstation for all four steps.

3. PLANAR INTERPOLATION

In the development of any interpolation strategy, the problem is to search for a field value at a point, from a discrete set of values. Thus, after regeneration of a finite element mesh, stress values at the Gauss points of the new mesh (destination field) must be interpolated from values known at the nodes of the old mesh (reference field).

In finite element analysis, unstructured meshes as used, consisting for example of six-node triangular elements with three Gauss points per element. For the six-node triangular element, the displacement field in the element is quadratic, and thus the stress field varies linearly. The stresses obtained are discontinuous between elements; that is, the values at the common edges (or points) between elements are not unique. In view of this feature, there are three planar interpolation methods available, as described below:

- (1) *Inverse Distance Algorithm (IDA)*. In this commonly used method, the values of the Gauss points in the reference field are summed using an inverse distance weighting function as

$$\phi_d = \frac{\sum (w_r \phi_r)}{\sum (w_r)} \quad (4)$$

where w_r is a weighting function defined as

$$w_r = d^{-e} \quad (5)$$

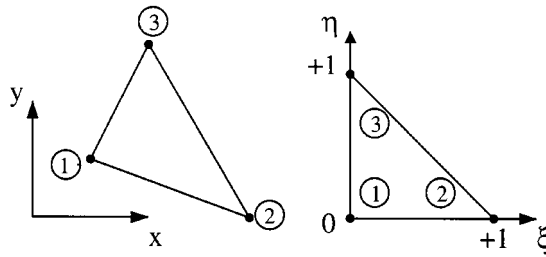


Figure 4. Numbering of Gauss points

in which d is the distance between points, and e is an exponent that is usually taken between 2 and 4, with 3.5 recommended.³⁷

In this simple method, a minimum value d for the distance between points may be specified. This will reduce the 'plateau' effects at each destination point, but the resulting interpolated field surface may not pass through the original reference field points.

- (2) *Arbitrary Linear Interpolation (ALI)*. Here, the three nearest reference Gauss points are found that surround a given destination Gauss point. Using these three old Gauss points as vertices, the stress values of the new Gauss point will be obtained from

$$\phi(\xi, \eta) = [1 - (\xi + \eta)] \phi_1 + \xi \phi_2 + \eta \phi_3 \quad (6)$$

where ξ and η are normalized local parameters (see Figure 4).

- (3) *Unique Element Method (UEM)*. This method is proposed to take account of the characteristics of the stress field in the six-node triangular mesh, which varies linearly within each element but with discontinuities between adjacent elements. The procedure is explained as:
- Updating the old mesh. The position of each node in the old mesh is updated by the cumulative displacements since the previous remeshing. This forms the reference field for interpolation.
 - Finding which element of the reference field the new Gauss point of the destination field lies in. During the preceding loading history, the boundary of the model domain will be deformed, and some distorted elements may appear. Using the new deformed boundary and the mesh generation method, the new mesh (destination field) is obtained. For each Gauss point in the destination field, it is necessary to establish in which element of the reference field it lies.
 - Interpolating or extrapolating the stress values at the new Gauss point (destination field). For each new Gauss point, the stresses are interpolated linearly (using equation (4)) from the three Gauss points of the old element in which the new Gauss point lies.

A comparison of the above three methods will be shown in the following section.

4. NUMERICAL SIMULATION

4.1. Numerical procedure

In the new numerical method, the mesh generation and interpolation algorithms have been implemented with the AFENA finite element package, which was developed at the Geotechnical

Research Centre, University of Sydney.³⁶ The solution procedure comprises:

- (a) mesh generation;
- (b) analysis of incremental displacements (AFENA) for a small number of steps;
- (c) mesh regeneration (or remeshing);
- (d) stress interpolation;
- (e) analysis of next set of incremental displacements (AFENA).

The cycle (c)–(e) is repeated until the desired settlement (or penetration) is reached.

4.2. Rough strip footing: effects of increment and mesh sizes

For illustration, the response of a rigid rough strip footing penetrating into homogeneous soil is analysed. The soil has been modelled by a simple elastic, perfectly plastic, Von Mises model. An undrained plane strain analyses is conducted, and the influence of different frequencies of remeshing is explored.

In these analyses, material properties have been taken as: Young's modulus, $E = 500$ kPa, cohesion $c = 1$ kPa, friction and dilation angles $= 0$, Poisson's ratio, $\nu = 0.49$. The soil weight is not considered, since it does not affect the results. The soil semi-field has been taken as 35 m wide and 20 m deep with a footing of semi-width 5 m, and a relatively coarse mesh adopted, as shown in Figure 5.

4.2.1. Effect of interpolation techniques. Figure 6 gives the load–settlement response obtained using IDA, ALI and UEM interpolation methods (where F is the computed vertical force; B is the semi-width of strip footing; and S is the settlement). The displacement increment was taken as $\delta(S/B) = 0.002$, and remeshing was implemented at every 10 increments, giving a remeshing interval of $\Delta(S/B) = 0.02$. It is apparent that the ALI method produces relatively large fluctuations after each remeshing; the IDA method is somewhat unstable, with sporadic large fluctuations among mainly small fluctuations; and the UEM method provides the steadiest and smoothest result. The large fluctuations in Figure 6 using the ALI, IDA and UEM interpolation methods are 13, 11 and 6.3 percent, respectively. It is clear therefore that the UEM method gives the smallest fluctuations. Moreover, the fluctuations are relatively regular using the UEM method; they are thus predictable and may be adjusted (see next section).

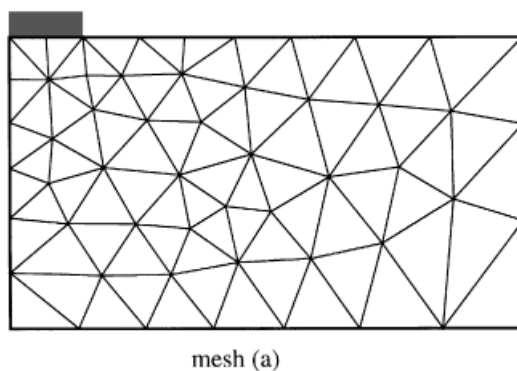


Figure 5. Coarse mesh for parametric study

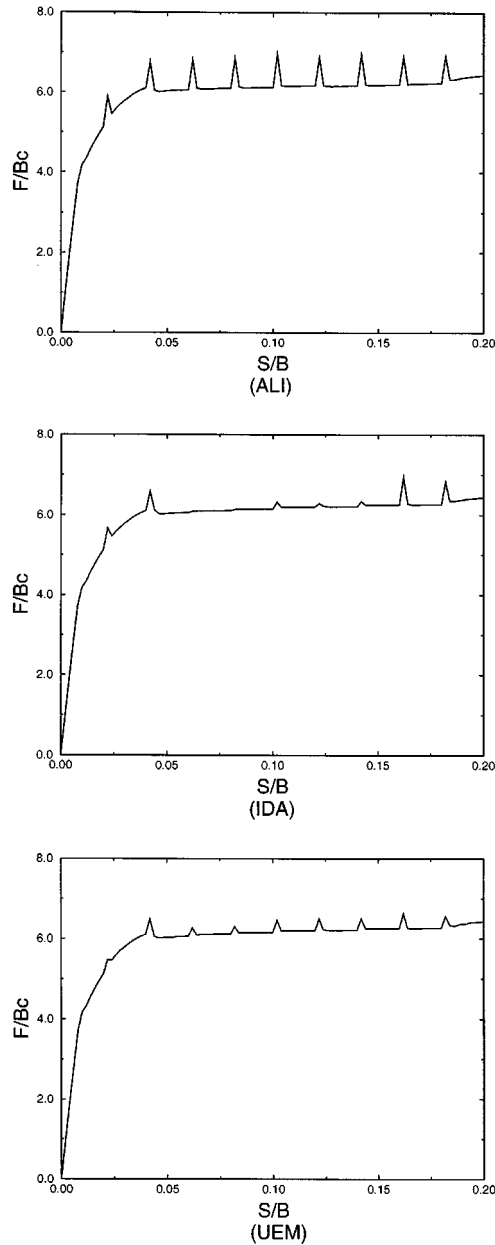


Figure 6. Comparison of three interpolation methods

The fluctuations that appear in the load–settlement deformation response with remeshing, result from the fact that nodal force equilibrium is disturbed during remeshing and interpolation. The ALI and IDA methods take the reference field as a smooth and continuous field, and consider neither element nor whole body equilibrium. Although the UEM method uses a unique

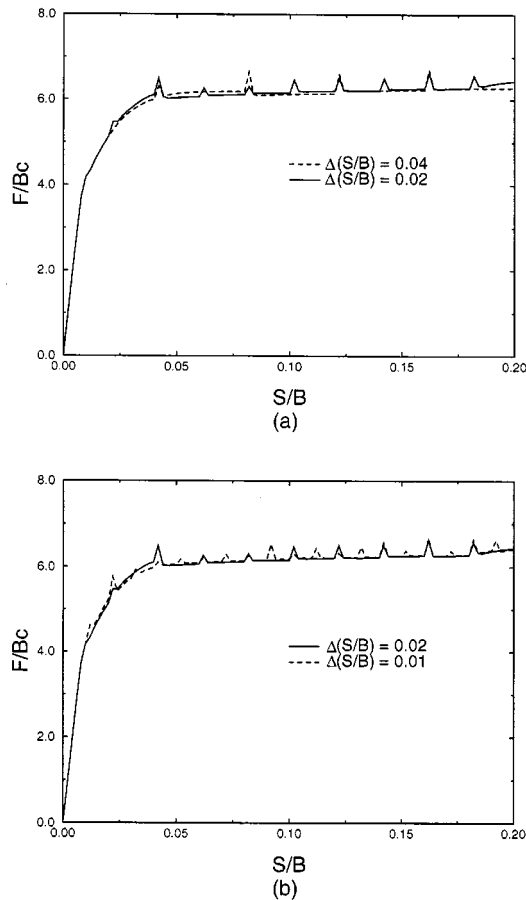


Figure 7. Load-settlement results using different remeshing intervals

element in the old field to interpolate the stresses of Gauss points in the new field, equilibrium of the whole body still cannot be guaranteed since Gauss points in any element of the new mesh may lie in different elements of the old mesh. However, the UEM method works better than the other two methods, and the overall load-deformation response is reasonably steady. An improved result could have been obtained using local patch techniques.³⁸ However, the additional computational effort would be considerable, and is not considered warranted.

4.2.2. Effect of mesh and remeshing. The accuracy of the solution is a function of the fineness of the mesh, and the size of the displacement or load increments. Figure 7 shows the load-settlement responses obtained using different intervals of remeshing $\Delta(S/B)$, but with the displacement increment kept constant at $\delta(S/B) = 0.002$. It can be seen that there is little difference in the amplitude of fluctuations for the three cases considered, and it may be concluded that the interval of remeshing does not have much effect on the amplitude of fluctuations. However, a too large

remeshing interval can lead to an unsteady load–settlement response, as seen for the largest interval of $\Delta(S/B) = 0.04$ (Figure 7(a)). For the two smaller remeshing intervals, the load–settlement responses are almost identical and steady (Figure 7(b)). Therefore it may be concluded that a remeshing interval of $\Delta(S/B) = 0.02$ is sufficient for the following analyses.

As mentioned above, the displacement increment $\delta(S/B)$ used was 0.002. The effect of different increments $\delta(S/B)$ on the computed load–settlement response is shown in Figure 8, maintaining a remeshing interval of $\Delta(S/B) = 0.02$. It can be seen that the increment size $\delta(S/B)$ primarily affects the amplitude of fluctuations. This is logical since smaller increments allow any out of balance forces following remeshing to be corrected more rapidly. Note that the size of the displacement increment has little effect on the overall load–settlement response.

The fineness of the mesh will also affect the results, because smaller elements size will give more accurate results. However, a finer mesh is more time consuming, especially when frequent remeshing is required. Figures 5 and 9 show the four different meshes used for comparison of results, with 188, 724, 1563 and 2352 nodes respectively. Figure 10 compares the load–settlement responses, taking $\Delta(S/B) = 0.02$ and $\delta(S/B) = 0.002$. It may be seen that mesh (c) and mesh (d) (Figure 9) give almost identical results, while for each remeshing cycle (each step of $\Delta(S/B)$), the corresponding CPU times were 635 and 1354 s, using a SUN Sparc-ELC. Given that the resulting responses are similar, mesh (c) is adequate. It may be pointed out that the element size just below the footing was 13 percent of the footing width for mesh (c), and 7 percent of the footing width for mesh (d).

From Figure 10, it is clear that the finest mesh leads to some unsteadiness in the ultimate bearing capacity, using a displacement increment of $\delta(S/B) = 0.002$. This is because the fine mesh needs a correspondingly smaller displacement increment for high accuracy, and halving the displacement increment leads once more to a smooth response.

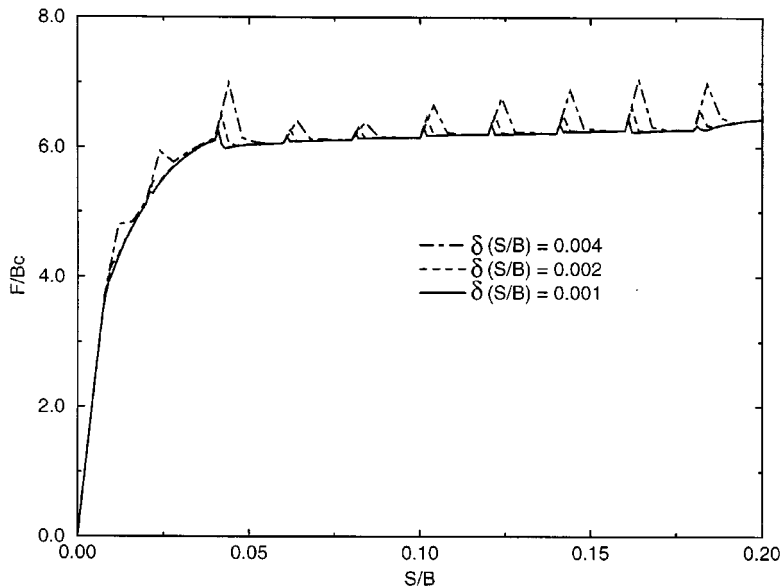


Figure 8. Effect of displacement increment on load–settlement response

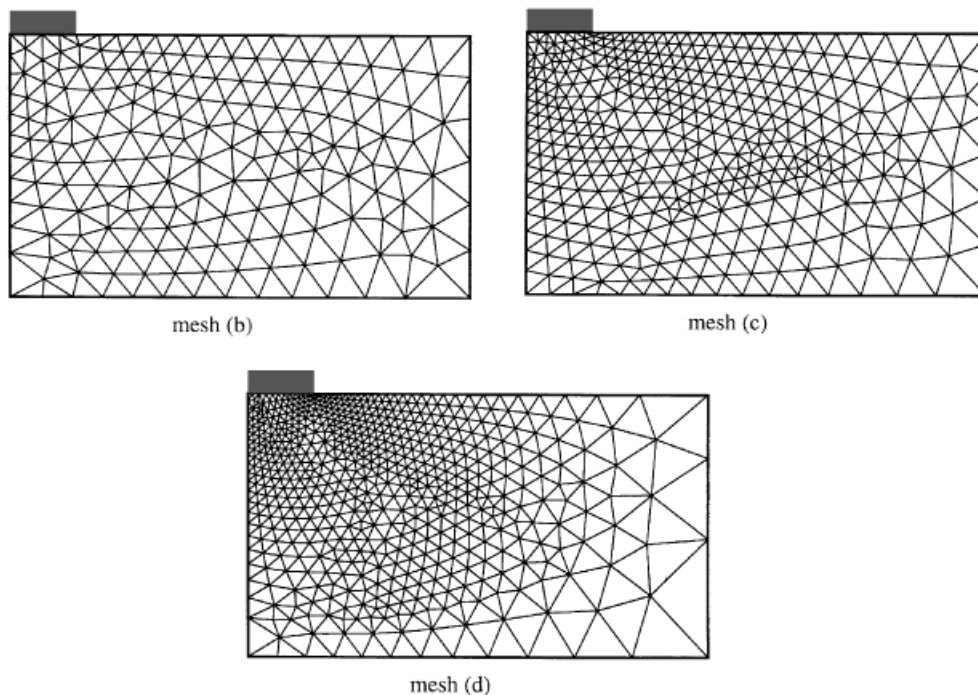


Figure 9. Meshes of different refinement

From plasticity theory, the ultimate bearing capacity of a strip footing is $F/(Bc) = 5.14$. The terminal bearing capacity factor in Figure 10 is 5.5. However, this reduces to 5.16 if the width of the strip is assumed to extend to half an element beyond the nodes that are constrained to move vertically downwards (a common adjustment).

4.2.3. Comparison of remeshing and no-remeshing results. A final comparison is included to illustrate the different load–settlement responses obtained with (a) no remeshing, (b) updating of mesh geometry by the displacement increments, and (c) full remeshing and interpolation. A displacement increment of $\delta(S/B) = 0.001$ and remeshing interval of $\Delta(S/B) = 0.01$ were adopted, with updating of the mesh in analysis (b) carried out after every displacement increment.

Figure 11 shows the three load–settlement responses. With no remeshing, the computed bearing capacity factor is $F/(Bc) = 5.5$ (again though, this reduces to 5.14 if the footing is assumed to extend half an element beyond the constrained nodes). For analysis (b), where the mesh is updated, the load–settlement response goes considerably higher than for the other two analyses. Figure 12 shows the updated mesh when $S/B = 0.2$. It is apparent that the elements around the footing edge are extremely distorted, leading to the poor result.

With remeshing, the regular fluctuations due to remeshing and interpolation have been filtered by taking only one data point in each interval of remeshing. The remeshing response agrees well with the result for no remeshing, up to a settlement of $S/B = 0.10$. Beyond that point, the difference between the two analyses becomes significant, as the bearing capacity is increased by material heaving to the side of the footing (an affect which can only be captured by the remeshing

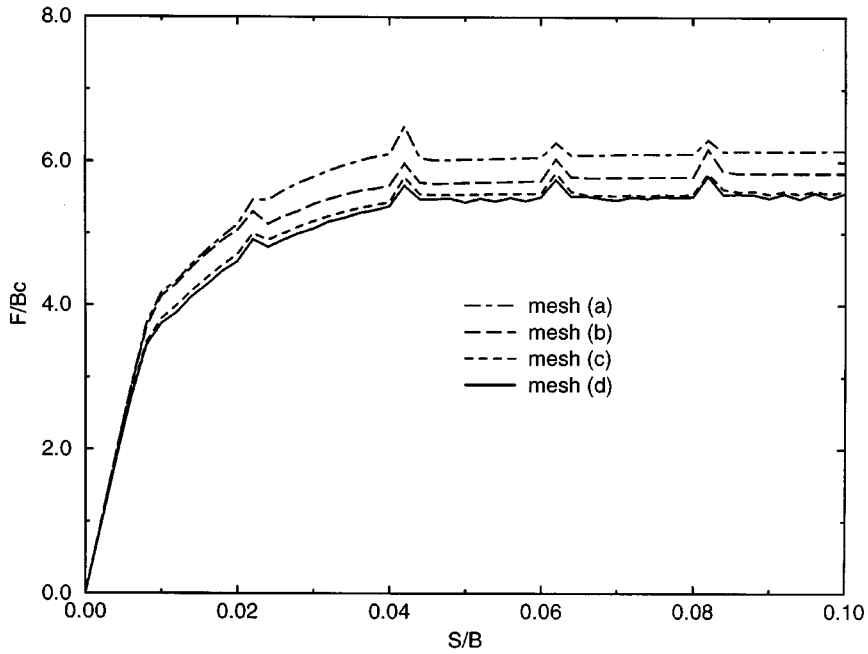


Figure 10. Effect of different meshes on load-settlement response

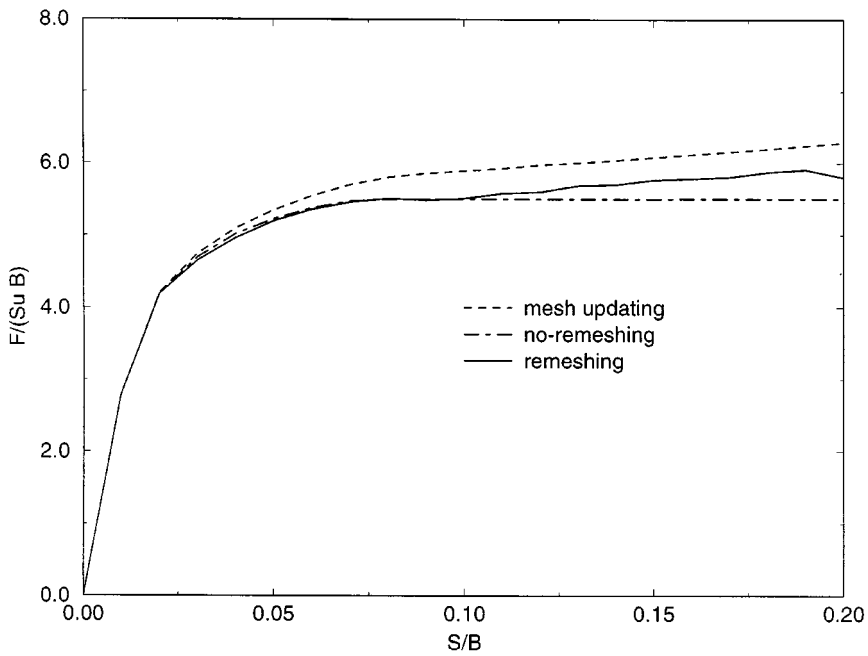


Figure 11. Comparison of computed responses with and without remeshing

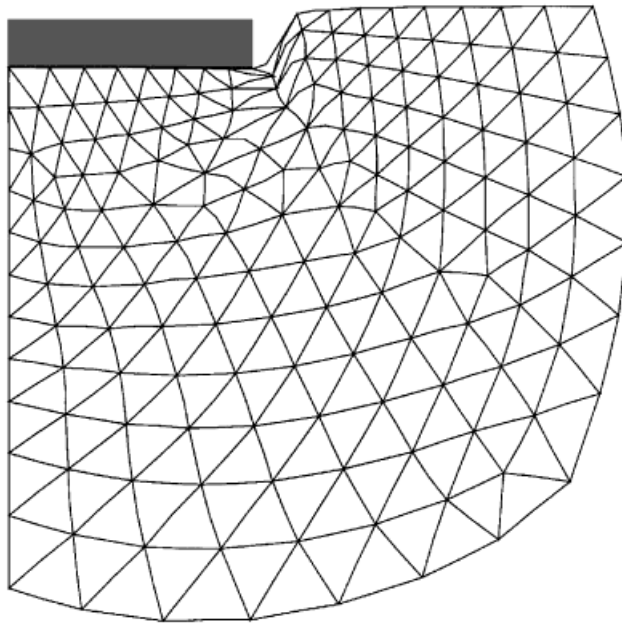


Figure 12. Deformed mesh using updated co-ordinates without remeshing

approach). It can also be seen that the load–settlement curve with remeshing shows slight unsteadiness, and indeed the load drops slightly just prior to a settlement of $S/B = 0.2$. This form of unsteadiness is linked to small changes in the detailed mesh, particularly near the edge of the footing, and reduces as the mesh is refined.

So far, the results presented have been for rather moderate settlements of up to 20 percent of the footing width. Two applications of the method are now presented where significant penetration of the foundation into soil occurs, and where the soil strength is assumed to increase linearly with depth.

4.3. Example application 1: cavity expansion

In order to validate the numerical method proposed in this paper, a large strain problem of cavity expansion is analysed in an elastic perfectly plastic soil. The soil properties are: uniform shear strength $s_u = 4 \text{ kPa}$, Young's modulus $E = 500s_u$ and Poisson's ratio $\nu = 0.49$. The soil self-weight and initial soil stresses are not considered in the calculation since they are not relevant.

Although cavity expansion is really a one-dimensional problem, it has been analysed here as a two-dimensional problem to test the present numerical method. Two analyses have been carried out: (a) a plain strain analysis of one quadrant from a horizontal slice through the cavity; and (b) an axisymmetric analysis. Figure 13(a) shows the quadrant domain used for the plain strain analysis with $R = 12 \text{ m}$, and Figure 13(b) shows the strip domain used in the axisymmetric analysis with $H = 0.5 \text{ m}$ and $R = 12 \text{ m}$. Elastic spring elements were used along the radial boundary of each domain, with stiffness $k = 2G/R$, in which $G = E/\{2*(1 + \nu)\}$ is the soil shear

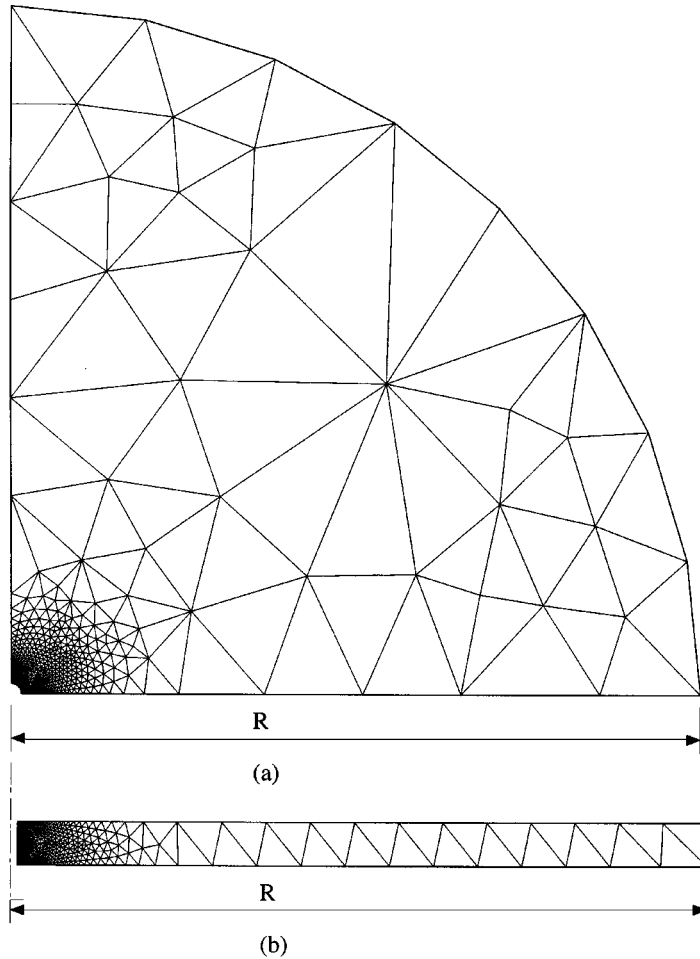


Figure 13. Meshes in cavity expansion analysis

modulus. Approximately 2700 nodes and 1000 six-noded triangular elements were used in both analyses.

In the analyses, remeshing was implemented for every 10 percent change of the cavity radius, with 20 increments between each remeshing stage. The initial cavity radius was $a_0 = 0.04$ m, and the cavity was expanded to $a = 0.20$ m, which is 5 times a_0 . The cavity wall pressure-displacement response is shown in Figure 14. The analytical solution⁴¹ is given by

$$p = s_u \{1 + \ln[(G/s_u)(1 - (a_0/a)^2)]\} \quad (7)$$

It is apparent that the numerical results and analytical solution agree extremely well. The numerical curve from the axisymmetric analysis is slightly higher than the analytical solution. This is because generally six-noded triangular elements do not predict limit loads well for axisymmetric analysis.⁴² However, if the mesh is fine enough, such elements appear to give

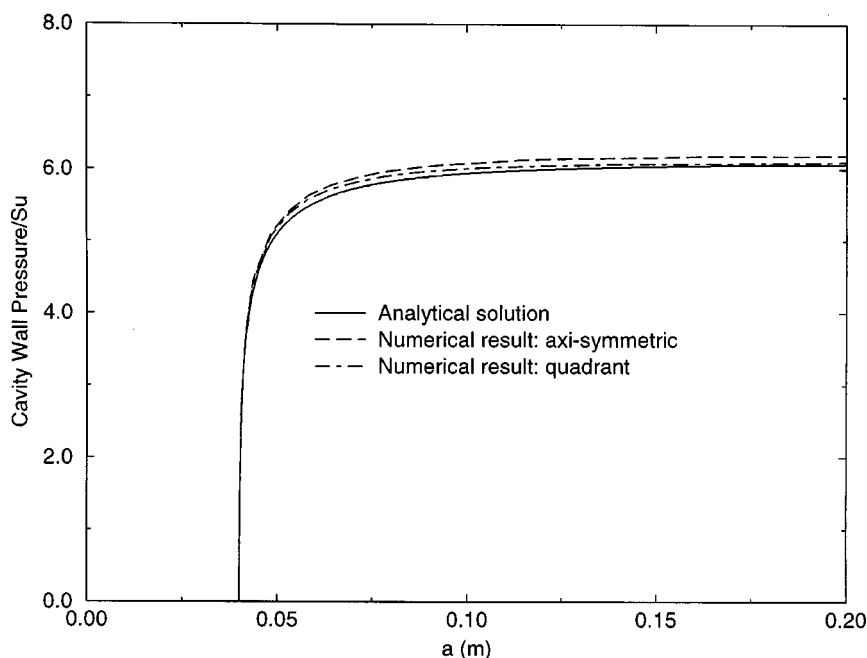


Figure 14. Cavity expansion response in elastic perfectly plastic soil

acceptable results. The plain strain analysis using the quadrant domain gives a slightly more accurate result.

This example demonstrates that there is no significant drift in the accuracy of the large strain solution, due to repeated remeshing.

4.4. Example application 2: strip footing

The penetration response of a strip footing of 10 m width (5 m semi-width) is analysed for soil with a strength profile given by $s_u = 1 + 2z \text{ kPa}$, where z is the depth below the ground surface. The soil has been modelled as an elastic, perfectly plastic Tresca material, with Young's modulus $E = 500s_u$ and Poisson's ratio $\nu = 0.49$. Results are presented for the case of weightless soil, and where the soil self-weight is 17 kN/m^3 . The foundation is assumed to be rectangular in elevation, with smooth sides.

Figure 15 shows the computed responses with (a) no remeshing (strip footing on the soil surface), (b) remeshing, with zero soil weight, and (c) remeshing, with soil weight of 17 kN/m^3 . Analytical solutions are shown, taken from Davis and Booker,³⁹ where the bearing capacity is given by

$$q_u = F_r(5.14s_u + 0.25kB) + \gamma z \quad (8)$$

where s_u is the soil strength at the current foundation penetration (depth of z), k is the rate of increase of shear strength with depth (2 kPa/m), B is the foundation width of 10 m and γ is the soil

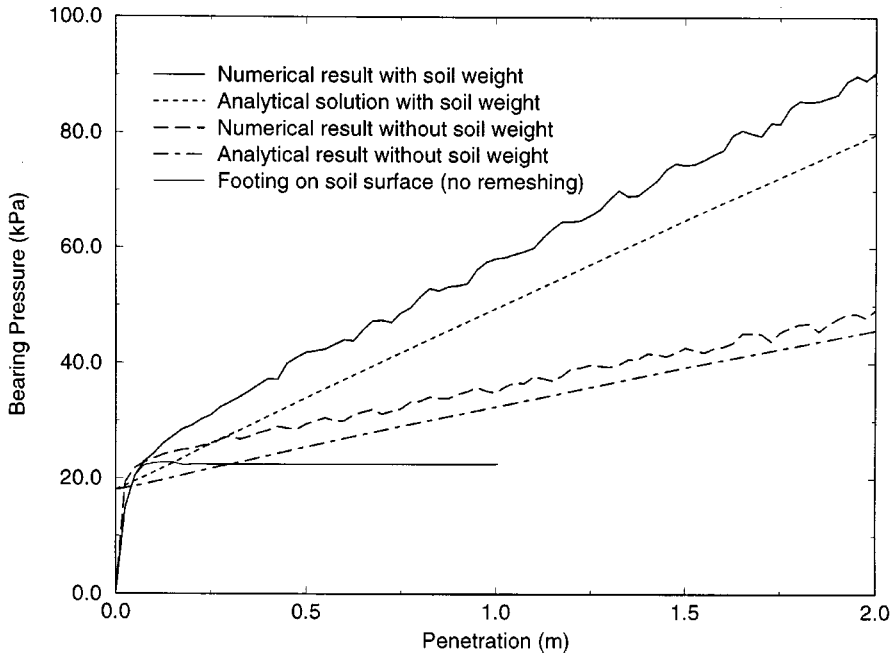


Figure 15. Response of strip footing on Tresca soil with strength increasing with depth

self-weight (0 or 17 kN/m^3). The factor F_r is given as a function of the relative strength gradient, kB/s_{u0} by Davis and Booker, where s_{u0} is the strength at the footing underside.

At the soil surface, the analytical bearing capacity is 18. kPa (a factor of 12.7 on the surface strength of 1 kPa). The computed responses show a bearing capacity at low penetration of about 22 kPa, on overprediction of about 20 percent (which may be reduced if the footing width is adjusted as discussed earlier). For the case of no soil self-weight, the computed bearing pressure stays consistently between 10 and 20 percent higher than the calculated value.

It should be noted that there are two compensating reasons for differences between the computed and calculated bearing capacities. The calculated bearing capacity ignores the contribution from the strength of the soil lying above the current plane of the footing (the Davis and Booker solution is for surface footings only). As such, the calculated capacity would be expected to fall progressively further below the computed value as the footing penetration increases.

However, the compensating difference is that the footing 'traps' soil of reduced strength directly beneath it, and this leads to a reduced computed bearing capacity. Figure 16 shows the distribution of shear strength down the line of symmetry beneath the footing, for a penetration of 2 m. The 'analytical' value assumes a linear increase from a value of 5 kPa at the footing surface, while the finite element profile shows a reduction to the original 1 kPa immediately below the footing.

Where self-weight is included, the computed bearing pressure stays some 20 percent above the calculated value, with full allowance for the beneficial effect of soil heave to the side of the footing. The effect of soil self-weight is clearly seen in the different surface profiles shown in Figure 17,

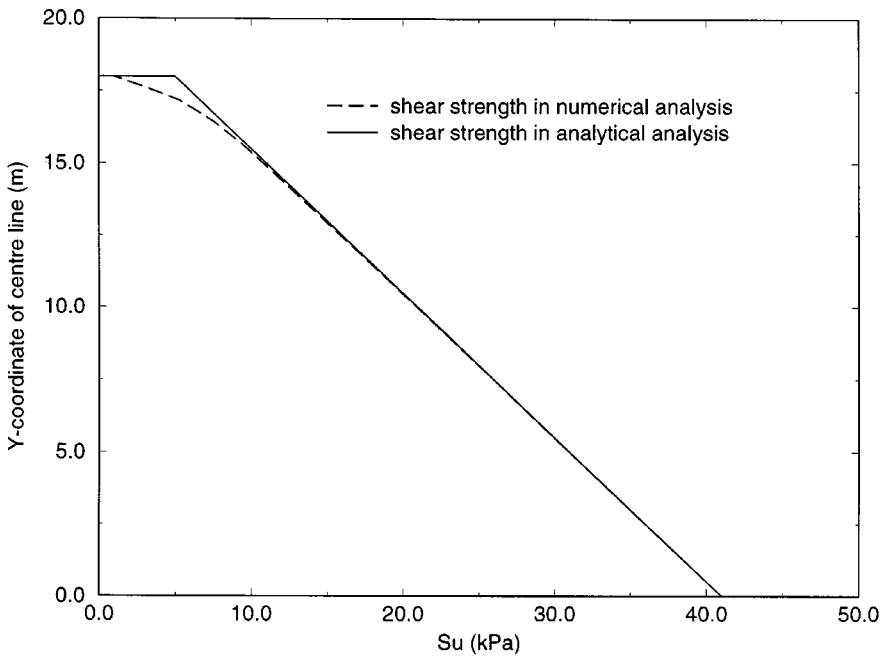


Figure 16. Profiles of soil shear strength down centre-line of footing

where the extent of the plastic region has been indicated by marking the Gauss points by a dot to indicate soil at yield. In the analysis with soil self-weight, the initial deviator stress (due to a K_0 of 0.5) leads to different development of the yielded zones.

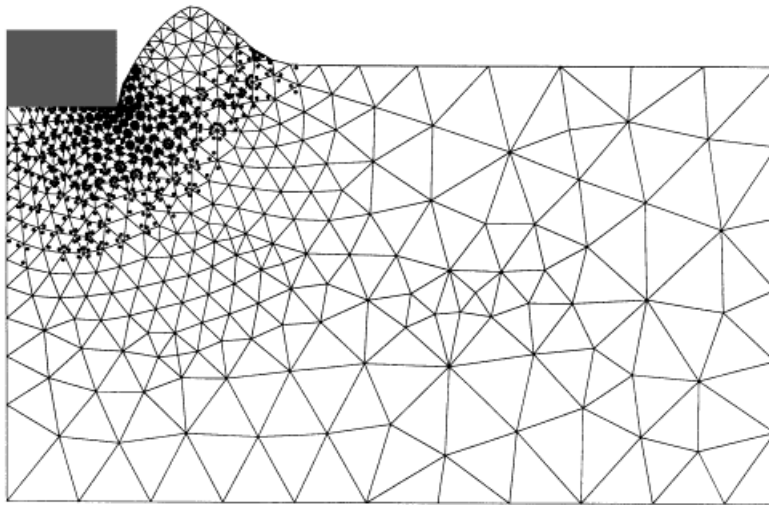
4.5. Example application 3: jack-up spudcan foundation

A final example is given, for a jack-up spudcan foundation of 14 m diameter (see Figure 18), penetrating into soil where the shear strength varies according to $s_u = 5.6 + 2z$ kPa. The strength intercept at the surface of 5.6 kPa has been adopted deliberately to allow comparison with lower bound solutions presented by Martin⁴⁰ for a 150° conical-based circular foundation penetrating soil where the relative strength gradient is $kD/s_{u0} = 5$, D being the diameter of the foundation.

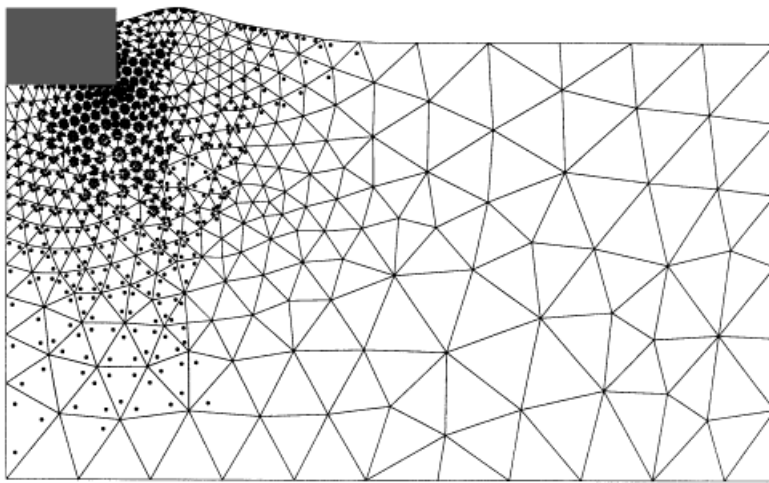
In the finite element analysis, the bottom 1.4 m of the spudcan tip has been truncated, in order to avoid the use of extremely small elements close to the actual tip. The base and sides of the spudcan have been assumed smooth.

Figure 19 shows that the computed response, with penetration shown relative to the extreme tip of the spudcan (a distance of 3.2 m below the bottom of the widest diameter of the foundation). Three separate forces are shown from the finite elements analysis, each expressed as an average pressure over the maximum cross-sectional area of the spudcan:

- (1) F_1 , the force on the bottom surface of the spudcan;
- (2) F_2 , the net force, as seen by the leg above the spudcan;



(a) Soil heave without soil self-weight



(b) Soil heave with soil self-weight

Figure 17. Soil heave with and without self-weight (2 m settlement of footing)

- (3) F_3 , the net force, F_2 , reduced further by the average 'buoyancy' due to the volume of the spudcan below the soil surface (on the basis that, if the spudcan was a thin plate, additional soil would have fallen back over the upper surface, reducing the net force); F_3 corresponds closest to the analytical case of a foundation penetrating weightless soil.

The analytical response shown in Figure 19 is taken from Martin.⁴⁰ It may be seen that the analytical response falls below the numerical result, due to the combined effect

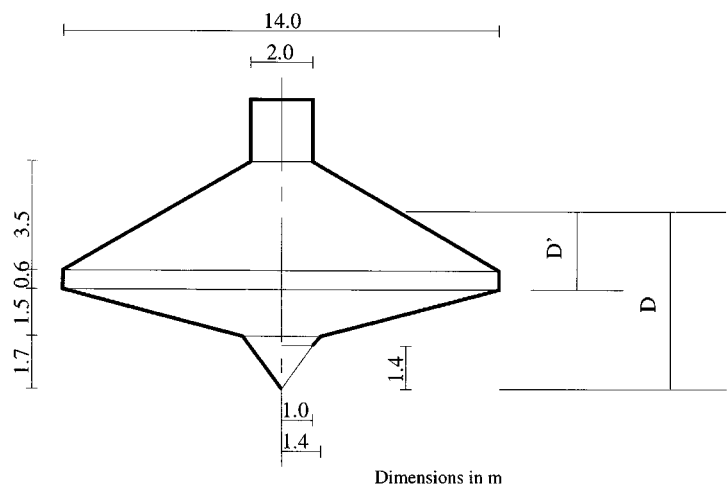


Figure 18. Geometry of spudcan

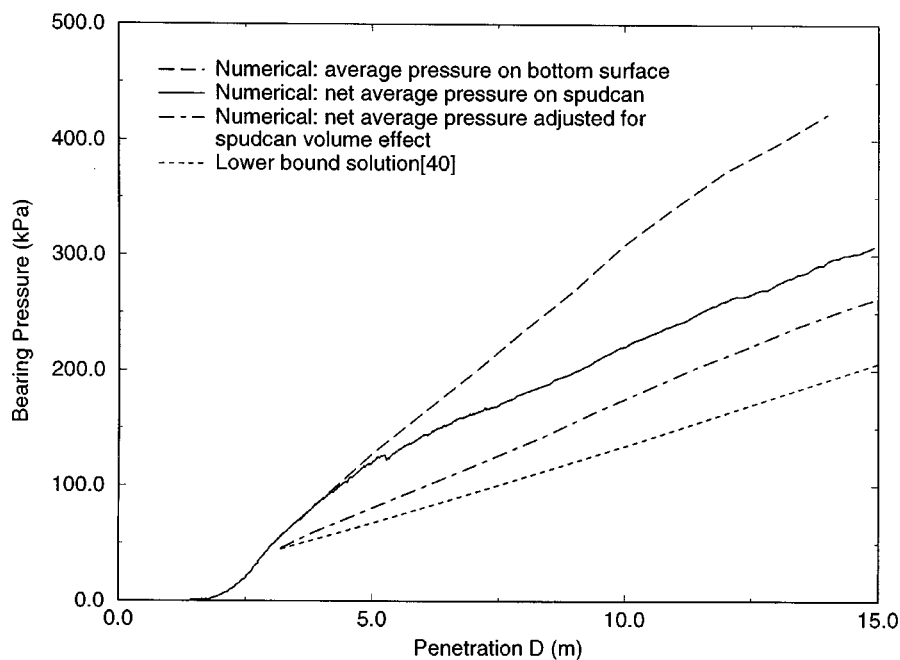


Figure 19. Deep penetration response of spudcan in soil with strength increasing with depth

of soil heave, and the strength of the soil lying above the plane of the spudcan. The effect of soil of low strength trapped below the spudcan is relatively small, due to the sloping base of the spudcan, and the assumption of smooth contact between the spudcan and the soil.

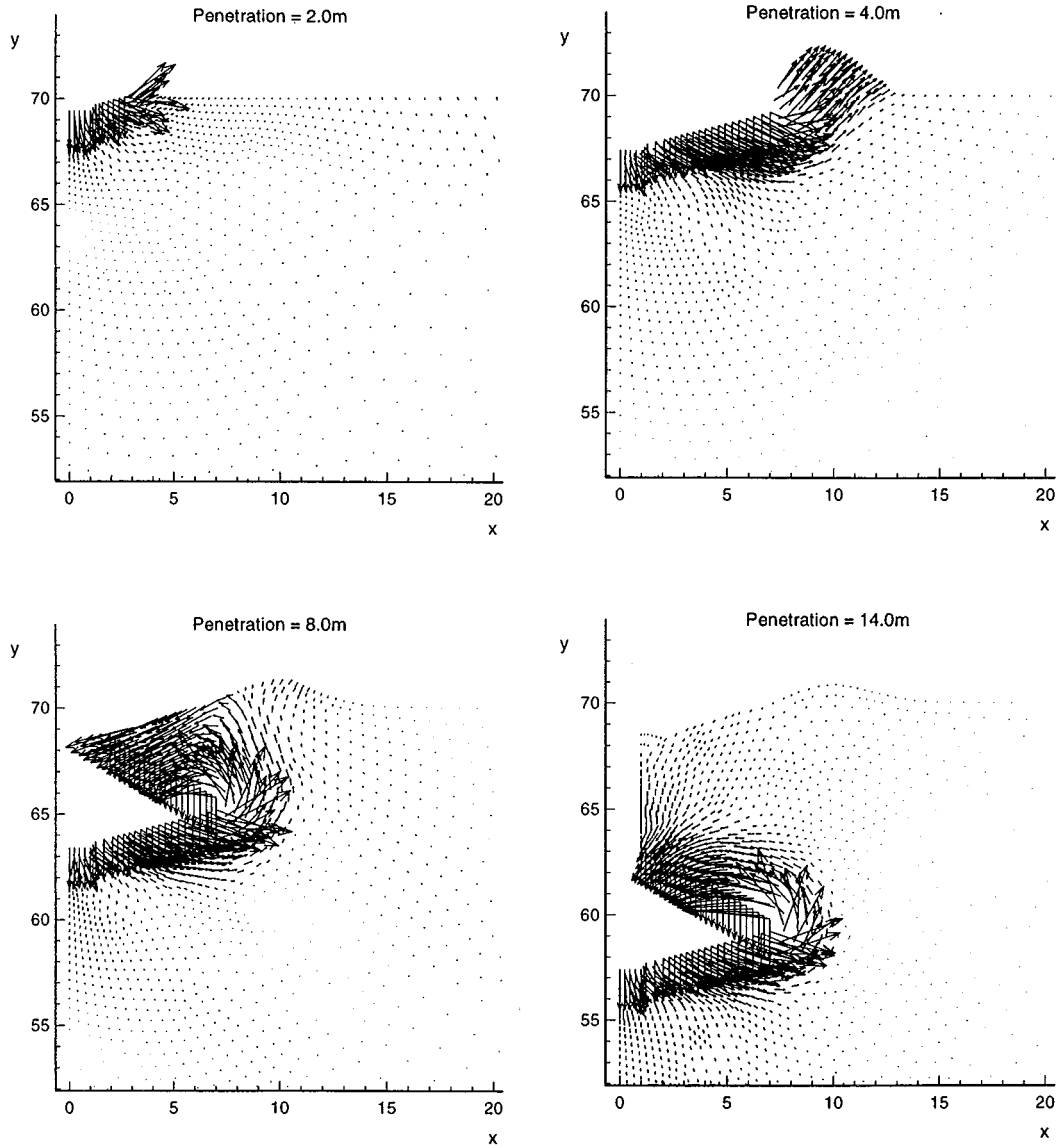


Figure 20. Incremental displacements at different stages of spudcan penetration

Figure 20 shows the incremental displacement vectors at four different stages of penetration of the spudcan (2, 4, 8 and 14 m, relative to the extreme tip). It may be seen that the soil flows around the spudcan, in a closely confined failure mode, with a small surface heave corresponding to the embedded volume of the spudcan.

5. CONCLUSIONS

Finite element analysis of problems involving large strains or deformations has traditionally involved rather complex formulations, based in either Eulerian (fixed mesh in space) or Lagrangian (mesh moving with body) approaches. Depending on the approach, additional terms such as second-order corrections to the strain relationships, to allow for rotation, or stress derivatives that allow for convection of material through the mesh, have needed to be added to the conventional small strain finite element equations.

The arbitrary Lagrangian–Eulerian (ALE) approach, decoupling nodal and material coordinates, was introduced in order to minimize the limitations associated with purely Lagrangian or Eulerian approaches. However, even with the formal ALE approach, additional terms were required in the finite element formulation.

The present paper presents a practical approach to finite element analysis of large deformation problems, based on the ALE concept, but without the need to modify the basic finite element equations. Instead, an efficient remeshing and interpolation technique is coupled with a conventional small strain finite element program. This approach is straightforward to implement, with the only overhead being the additional computational resources required for the remeshing and interpolation steps.

A fast and robust remeshing strategy, based on normal offsetting of nodes from the domain boundary, Delaunay triangulation and Laplacian smoothing, is described, with the mesh density being determined by a simple distance function. In principle, it is straightforward to extend this technique to adaptive mesh generation, with the density function linked to strain gradients or measures of errors in the finite element analysis.

A direct planar interpolation for stress and material properties, based on the unique element method, has been shown to provide adequate accuracy, with only minor fluctuations introduced in overall equilibrium. This approach is a good compromise between simplicity (and hence computational cost) and reasonable accuracy, compared with more accurate patch techniques that would have a much higher computational overhead.

The method has been applied to problems in soil mechanics involving surface penetration of plane strain and axisymmetric foundations. A full parametric study is included where the effects of displacement increment, remeshing frequency, and mesh refinement are explored. It is shown that good accuracy is obtained with displacement increments of 0.1 to 0.2 percent of the foundation semi-width (or radius), and remeshing every 10–20 increments.

The computed load-penetration responses have been compared with calculations of bearing capacity based on plasticity approaches, and have been shown to offer an accuracy within about 10 percent. In the final example, the challenging problem of deep penetration of a jack-up spudcan foundation, in soil where the strength varies linearly with depth, is addressed. The proposed finite element method is shown to model well the flow of soil back over the upper surface of the foundation, and to provide an overall load-penetration response that is similar to, but some 20 percent higher than, the bearing capacity profile calculated using a conventional approach based on plasticity solutions.

In summary, the proposed finite element formulation provides a practical approach that can make full use of well-established small strain finite element codes, and yet is able to offer accurate solution of challenging problems in soil mechanics that involve large strains and deformations.

ACKNOWLEDGEMENTS

The work described in this paper is part of a research programme into the response of offshore foundations, supported by the Australian Research Council. This support is gratefully acknowledged. Thanks are also due to Professor John Carter and Associate Professor Scott Sloan for providing source code of finite element and triangulation routines.

7. REFERENCES

1. C. Truesdell, *A First Course In Rational Mechanics, Vol. 1: General Concepts*, Academic Press, New York, 1977.
2. S. Ghosh and N. Kikuchi, 'An arbitrary Lagrangian–Eulerian finite element method for large deformation analysis of elastic-viscoplastic solid', *Comput. Meth. Appl. Mech. Engng.*, **86**, 127–188 (1991).
3. M. S. Gadala, G. A. E. Oravas and M. A. Dokainish, 'A consistent Eulerian formulation of large deformation problems in statics and dynamics', *Int. J. Non-linear Mech.*, **18**, 21–35 (1983).
4. P. van den Berg, 'Numerical model for cone penetration', *Proc. Int. Conf. on Comput. Methods Adv. Geomechanics*, **3**, 1777–1782 (1991).
5. M. S. Gadala, G. A. E. Oravas and M. A. Dokainish, 'A consistent eulerian formulation of large deformation problems in statics and dynamics', *Int. J. Non-linear Mech.*, **18**, 21–35 (1983).
6. O. C. Zienkiewicz, 'Flow formulation for numerical solution of forming processes', in J. F. T. Pittman et al. (eds), *Numerical Analysis of Forming Processes*, Wiley, New York, 1984, pp. 1–44.
7. J. H. Cheng and N. Kikuchi, 'A mesh rezoning technique for finite element simulations of metal forming processes', *Int. J. Numer. Meth. Engng.*, **23**, 219–228 (1986).
8. S. Ghosh, 'Finite element simulation of some extrusion processes using the arbitrary Lagrangian–Eulerian description', *ASM Int. J. Mater. Shaping Technol.*, **8**, 53–64 (1990).
9. S. Ghosh, 'Arbitrary Lagrangian–Eulerian finite element analysis of large deformation in contacting bodies', *Int. J. Numer. Meth. Engng.*, **33**, 1891–1925 (1992).
10. R. B. Haber, 'A mixed Eulerian–Lagrangian displacement model for large deformation analysis in solid mechanics', *Comput. Meth. Appl. Mech. Engng.*, **43**, 277–292 (1984).
11. W. K. Liu, T. Belytschko and H. Chang, 'An arbitrary Lagrangian–Eulerian finite element method for path dependent materials', *Comp. Meth. Appl. Mech. Engng.*, **58**, 227–245 (1986).
12. W. K. Liu, H. Chang, J. S. Chen and T. Belytschko, 'Arbitrary Lagrangian–Eulerian Petrov–Galerkin finite elements for nonlinear continua', *Comput. Meth. Appl. Mech. Engng.*, **68**, 259–310 (1988).
13. J. Huetink, J. van der Lugt and P. T. Vreede, 'A mixed Euler–Lagrangian finite element method for simulation of thermo-mechanical processes', in J. L. Chenot and E. Onate (eds), *Modelling of Metal Forming Processes*, Kluwer, 1988, pp. 57–64.
14. P. D. Kioussis, G. Z. Voyiadjis and M. T. Tumay, 'A large strain theory for two dimensional problems in geomechanics', *Int. J. Numer. Anal. Meth. Geomech.*, **10**(1), 17–39 (1986).
15. P. D. Kioussis, G. Z. Voyiadjis and M. T. Tumay, 'A large strain theory and its application in the analysis of the cone penetration mechanism', *Int. J. Numer. Anal. Meth. Geomech.*, **12**, 45–60 (1988).
16. P. van den Berg, J. A. M. Teunissen and J. Huetink, 'Cone penetration in layered media, an ALE element formulation', *Proc. Int. Conf. on Computer Methods and Advances in Geomechanics*, Vol. 3, 1991, pp. 1957–1962.
17. K. Ho-Le, 'Finite element mesh generation method: a review and classification', *Comput. Aided Desg.*, **20**, 27–38 (1988).
18. J. Suhara and J. Fukuda, 'Automatic mesh generation for finite element analysis', in *Advances in Computational Methods in Structural Mechanics and Design*, UAH Press, USA, 1972.
19. J. C. Gavendish, 'Automatic triangulation of arbitrary planar domains for the finite element method', *Int. J. Numer. Meth. Engng.*, **8**, 679–696 (1974).
20. A. O. Moscardini, B. A. Lewis and M. Cross, 'AGTHOM automatic generation of triangular and higher order meshes', *Int. J. Numer. Meth. Engng.*, **19**, 1331–1353 (1983).
21. R. D. Shaw and R. G. Pitchen, 'Modifications to the Suhara–Fukuda method of network generation', *Int. J. Numer. Meth. Engng.*, **12**, 93–99 (1978).
22. S. H. Lo, 'A new mesh generation scheme for arbitrary planar domains', *Int. J. Numer. Meth. Engng.*, **21**, 1403–1426 (1985).
23. Y. T. Lee, 'Automatic finite element generation based on constructive solid geometry', *Ph.D. Thesis*, Mechanical Engineering Dept, University of Leeds, 1983.
24. W. C. Thacker, A. Gonzalez and G. E. Putland, 'A method for automating the construction of irregular computational grids for storm surge forecast models', *J. Comput. Phys.*, **37**, 371–387 (1980).
25. N. Kikuchi, 'Adaptive grid-design methods for finite element analysis', *Comput. Meth. Appl. Mech. Engng.*, **55**, 129–160 (1986).

26. H. Samet, 'The quadtree and related hierarchical data structures', *ACM Comput. Surveys*, **16**(2), 187–260 (1984).
27. S. F. Yeung and M. B. Hsu, 'A mesh generation method on set theory', *Comput. Struct.*, **3**, 1063–1077 (1973).
28. R. Haber, M. S. Shephard, J. F. Abel, R. H. Gallagher and D. P. Greenberg, 'A general two-dimensional graphical finite element preprocessor utilizing discrete transfinite mappings', *Int. J. Numer. Meth. Engng.*, **17**, 1015–1044 (1981).
29. H. D. Cohen, 'A method for the automatic generation of triangular elements on a surface', *Int. J. Numer. Meth. Engng.*, **15**, 470–476 (1980).
30. A. Bykat, 'Design of a recursive, shape controlling mesh generator', *Int. J. Numer. Meth. Engng.*, **9**, 1357–1390 (1983).
31. E. A. Sadek, 'A scheme for the automatic generation of triangular finite elements', *Int. J. Numer. Meth. Engng.*, **15**, 1813–1822 (1980).
32. D. A. Lindholm, 'Automatic triangular mesh generation on surface of polyhedra', *IEEE Trans. Mag.*, **19**(6), 1539–1542 (1983).
33. B. P. Johnston and J. M. Sullivan, 'Fully automatic two dimensional mesh generation using normal offsetting', *Int. J. Numer. Meth. Engng.*, **33**, 425–442 (1992).
34. S. W. Sloan, 'A constrained Delaunay triangulation algorithm for generating finite element meshes', *Proc. Int. Conf. for Comp. Meth. Adv. Geomech.*, Cairns, Vol. 1, 1991, pp. 113–118.
35. L. R. Herman, 'Laplacian-isoparametric grid generation scheme', *J. Engng. Mech. Div. ASCE*, **102**, 749–759 (1976).
36. J. P. Carter and N. Balaam, *AFENA Users Manual*, Geotechnical Research Centre, The University of Sydney, 1990.
37. *TECPLOT version 5 Users Manual*, Amtec Engineering, Western Australia, 1992.
38. O. C. Zienkiewicz and J. Z. Zhu, 'The superconvergent patch recovery and a posteriori error estimates. Part 1: The recovery technique', *Int. J. Numer. Meth. Engng.*, **33**, 1331–1364 (1992).
39. E. H. Davis and J. R. Booker, 'The effect of increasing strength with depth on the bearing capacity of clays', *Geotechnique*, **23**(4), 551–563 (1973).
40. C. M. Martin, 'Physical and numerical modelling of offshore foundations under combined loads', *Ph. D. Thesis*, The University of Oxford, 1994.
41. B. G. Clarke, *Pressuremeters in Geotechnical Design*, Blackie Academic, Glasgow, 1995.
42. S. W. Sloan and M. F. Randolph, 'Numerical prediction of collapse loads using finite element methods', *Int. J. Numer. Anal. Meth. Geomech.*, **6**, 47–76 (1985).